Available online at www.sciencedirect.com
SCIENCE DIRECT®
Journal of Hydrology 281 (2003) 36–54
Journal of Hydrology
www.elsevier.com/locate/jhydrol

Steady-state analysis of cross-hole pneumatic injection tests in unsaturated fractured tuff

Walter A. Illman[a,*], Shlomo P. Neuman[b]

[a]*Department of Geoscience, The University of Iowa, Iowa City, IA 52242, USA*
[b]*Department of Hydrology and Water Resources, The University of Arizona, Tucson, AZ 85721, USA*

Received 24 April 2002; accepted 1 May 2003

Abstract

Numerous single-hole and cross-hole pneumatic injection tests have been conducted in unsaturated fractured tuff at the Apache Leap Research Site (ALRS) near Superior, Arizona. Steady-state analyses of single-hole tests conducted by Guzman et al. [Summary of Air Permeability Data From Single-Hole Injection Tests in Unsaturated Fractured Tuffs at the Apache Leap Research Site: Results of Steady-State Test Interpretation (1996)] have yielded values of air permeability at various locations throughout the tested rock volume on nominal scales from 0.5 to 3.0 m. Analyses of transient data from single-hole and larger-scale cross-hole tests were performed by Illman and Neuman [Ground Water 38 (2000) 899; Water Resour. Res. 37 (2001) 583] using type-curves and by Vesselinov and Neuman [Ground Water 39 (2001) 685] and Vesselinov et al. [Water Resour. Res. 37 (2001a) 3001; Water Resour. Res. 37 (2001b) 3041] using numerical inversion. These have yielded bulk fracture permeabilities and porosities on scales ranging from a few meters to several tens of meters. We complement the latter results by steady-state analysis of a relatively large set of cross-hole tests. Steady-state analysis (a) allows interpreting cross-hole tests that were not interpreted using type-curves due to weak or noisy signals, (b) is relatively easy to perform, and (c) yields results comparable with those obtained from transient analyses. We analyze the results statistically and discuss their implications vis-a-vis the pneumatic properties of unsaturated fractured tuff at the ALRS. Our results strengthen the evidence for a previously surmised permeability scale effect at the site.

Keywords: Permeability; Fractures; Tuff; Tomography; Unsaturated zone; Statistical analysis

1. Introduction

The characterization of unsaturated fractured rocks by means of hydraulic tests is fraught with logistical and technical difficulties. Many of these difficulties can be overcome by conducting field tests with air rather than with water (Kirkham, 1946; Boardman and Skrove, 1966; Montazer, 1982; Trautz, 1984; Mishra et al., 1987; Rasmussen et al., 1990, 1993; Baehr and Hult, 1991; Edwards and Jones, 1994; Massmann and Madden, 1994; LeCain and Walker, 1994; LeCain, 1995, 1996, 1998; Guzman et al., 1996; Illman et al., 1998; Wang et al., 1998; Huang et al., 1999; Benito et al., 1998, 1999).

Numerous single-hole (Guzman et al., 1994, 1996) and cross-hole (Illman et al., 1998; Illman, 1999)

* Corresponding author. Tel.: +1-3193351827; fax: +1-3193351821.
E-mail address: walter-illman@uiowa.edu (W.A. Illman).

0022-1694/03/$ - see front matter © 2003 Elsevier B.V. All rights reserved.
doi:10.1016/S0022-1694(03)00199-9

pneumatic injection tests have been conducted by the University of Arizona at the Apache Leap Research Site (ALRS) near Superior, Arizona. The tests were conducted in vertical and inclined (at 45°) boreholes drilled to a maximum depth of 30 m in unsaturated, slightly welded fractured tuff. Guzman et al. (1994, 1996) and Guzman and Neuman (1996) conducted over 270 single-hole pneumatic injection tests in short isolated intervals within six boreholes. By considering relatively stable periods of injection rate and pressure during each test, the authors were able to estimate the bulk permeability of fractures within the surrounding rock on nominal scales of 0.5–3.0 m by means of steady-state formulae. Analyses of transient data from a selected number of single-hole tests were performed by Illman and Neuman (2000) using type-curves, and by Vesselinov and Neuman (2001) using a numerical inverse model. These analyses have yielded estimates of bulk fracture permeability, porosity, skin factor and dimensionality of the flow regime on a nominal scale of 1 m.

Single-hole pneumatic injection tests provide information only about a small volume of rock in the close vicinity of the injection interval. Fractured rock properties measured on such small scales tend to vary rapidly and erratically in space so as to render the rock strongly and randomly heterogeneous. To determine the properties of the rock on larger scales, Illman et al. (1998) and Illman, (1999) have conducted numerous cross-hole pneumatic injection tests at the site. The tests were conducted by injecting air into an isolated interval within one borehole while monitoring pressure responses in isolated intervals within this and other boreholes. Analyses of transient data from one of these cross-hole tests were performed by Illman and Neuman (2001) using type-curves, and from several tests by Vesselinov et al. (2001a,b) using numerical inversion. These analyses have yielded bulk fracture permeabilities and porosities on scales ranging from a few meters to several tens of meters.

Tests, during which injection took place in low to moderate permeability intervals, proved to be more difficult to analyze by means of transient methods than those during which injection took place in high permeability intervals. This is so because the latter tests have generated distinct pressure signals that were relatively unaffected by background noise (due in large part to atmospheric pressure fluctuations) whereas the former tests have generated relatively weak pressure signals that were more difficult to separate from noise.

There have been no previous steady-state analyses of cross-hole test data from the ALRS. We present such analyses in this paper for a larger set of cross-hole tests than those analyzed previously by transient methods. In particular, we include in our analysis data from tests during which injection took place into intervals of low to moderate permeability. These tests have yielded relatively weak signals that would have been difficult to interpret by transient methods. The interpretation of transient data is further complicated by factors such as non-linear borehole and rock storage effects due to the large compressibility of air, and borehole skin effects. These factors have a much lesser impact on parameter estimates obtained on the basis of steady-state data. Though steady-state analyses do not yield information about fracture porosities, we expect them to provide reliable estimates of bulk fracture permeabilities. We analyze our results statistically and discuss their implications vis-a-vis the pneumatic properties of unsaturated fractured tuff at the ALRS. Our results provide further evidence for a previously surmised permeability scale effect at the site (Illman and Neuman, 2001; Vesselinov et al., 2001a,b; Hyun et al., 2002).

2. Site description

The ALRS is located near Superior, Arizona, at an elevation of 1200 m above mean sea level (Fig. 1). It is situated near Apache Leap, a 600 m west-facing escarpment that exposes a thick layer of volcanic tuff and underlying carbonates. The tuff is a consolidated ash-flow sheet of dacite that has its origin in a turbulent mixture of hot gas and pyroclastic material about 19 million years ago. The ash-flow sheet (Peterson, 1961) covers an area of 1000 km^2 and varies considerably in thickness about an average of 300 m. Climate at the site is warm-temperate and semi-arid, with a mean annual precipitation of less than 500 mm. Precipitation occurs primarily from mid-July to late-September in the form of high

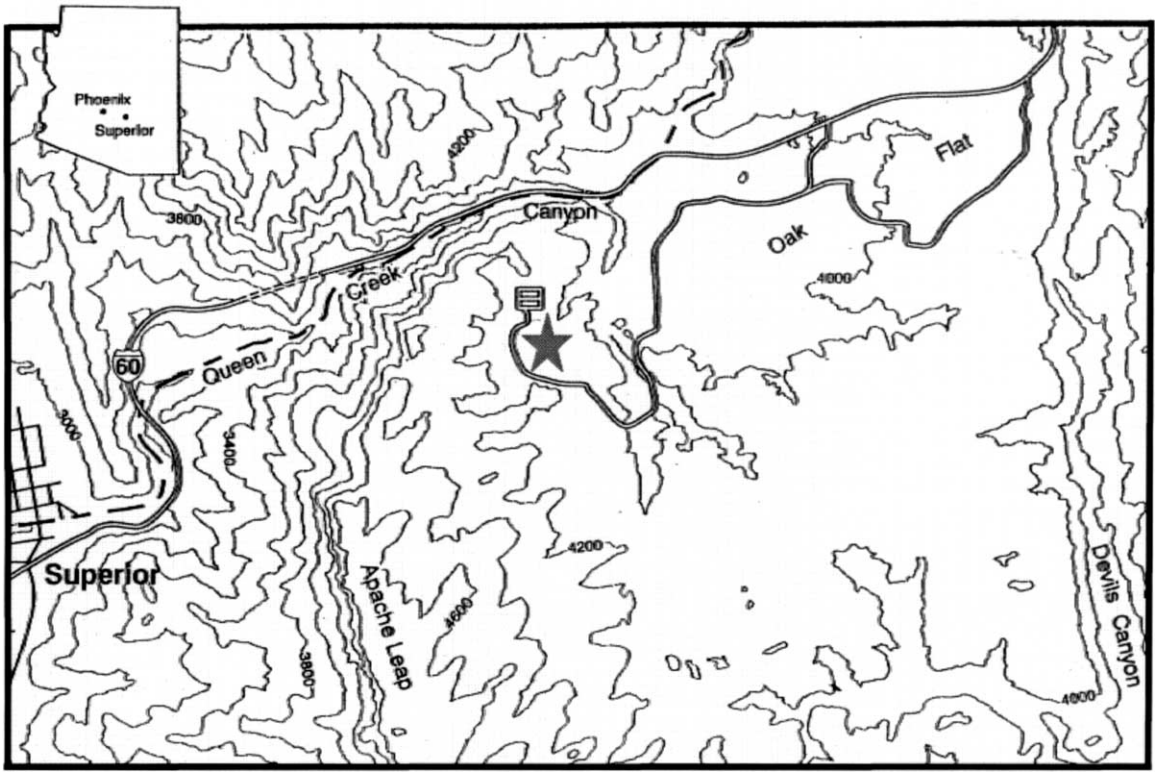

Fig. 1. Location map of ALRS test area (star). Elevation contours are in feet above mean sea level.

intensity, short duration thunderstorms, and from mid-November to late-March as rains of longer duration and lower intensity. The regional water table lies at a variable depth of more than 600 m. Except for a relatively thin perched zone of saturation at a depth of approximately 150 m, the rock above the water table is unsaturated.

The test site included 22 vertical and inclined (at 45°) boreholes that have been completed to a maximum depth of 30 m within a geologically distinct unit of partially welded unsaturated tuff. A three-dimensional perspective of the boreholes at the site is shown in Fig. 2. The upper 1.8 m of each borehole was cased. Cross-hole testing was conducted in 16 boreholes belonging to the sets V, W, X, Y and Z, which span a volume of rock on the order of 60,000 m^3. A surface area of approximately 1200 m^2 was covered with a thick plastic sheet to minimize infiltration and evaporation before and during pneumatic tests. Additional details of the site are given by Illman et al. (1998).

3. Previous work at the ALRS

Early work related to our area of study at the ALRS is described by Trautz (1984), Rasmussen and Evans (1987, 1989, 1992), Tidwell et al. (1988), Yeh et al. (1988), Weber and Evans (1988), Chuang et al. (1990), Rasmussen et al. (1990, 1993, 1996), Evans and Rasmussen (1991), Haldeman et al. (1991) and Bassett et al. (1994). This work included drilling, the retrieval of oriented core samples totaling 270 m in length, geophysical logging and televiewer imaging of the boreholes, and a variety of field and laboratory tests. Laboratory measurements on core samples provided information about rock matrix interstitial properties such as bulk density, effective porosity, skeletal density, pore surface area, and pore size distribution; hydraulic properties such as saturated and unsaturated hydraulic conductivity and moisture retention characteristics; pneumatic properties such as oven-dry and unsaturated air-phase

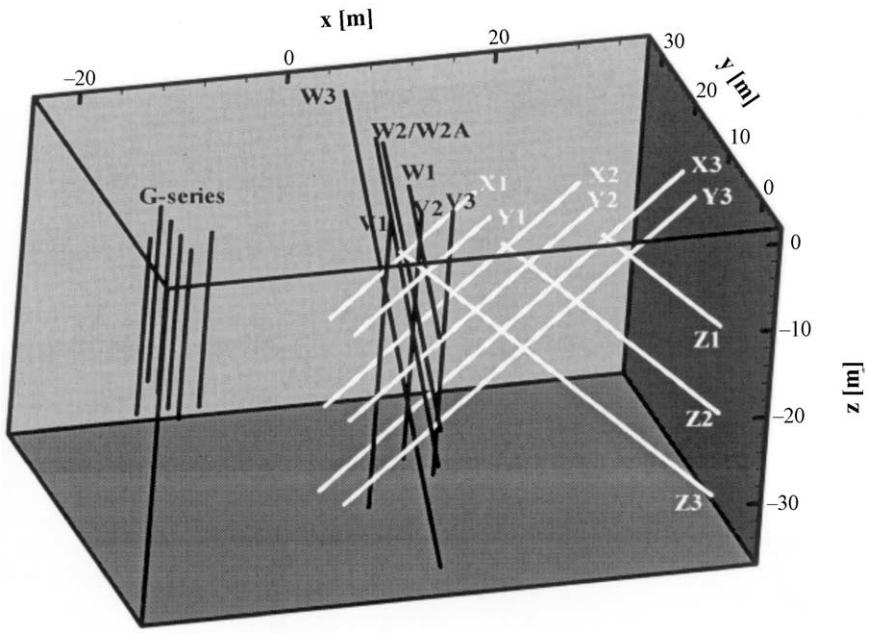

Fig. 2. Three-dimensional perspective of the boreholes at the site.

permeability; and Klinkenberg slip flow coefficient (Klinkenberg, 1941).

Information about the location and geometry of fractures has been obtained from surface observations, the examination of oriented cores, and borehole televiewer records. A summary of data concerning the orientation, dip and density of fractures in boreholes can be found in Rasmussen et al. (1990). A total of 79 fractures have been identified in boreholes at the site. The fractures appear to be exponentially distributed in a manner consistent with a Poisson process of fracture locations. Fracture density, defined by Rasmussen et al. (1990) as number of fractures per meter in a 3 m borehole interval, ranges from zero to a maximum of 4.3 per meter. The fractures exhibit a wide range of inclinations and trends, but most are near vertical and strike north–south. Vickers et al. (1992) reported a study of aperture distribution in a large natural fracture at the site.

Single-hole pneumatic injection tests were conducted in 87 intervals of 3 m length in nine boreholes by Rasmussen et al. (1990, 1993). According to Rasmussen et al. (1993), the tests were conducted by injecting air at a constant injection rate between two inflated packers while monitoring pressure within the injection interval. Pressure was said to have reached stable values within minutes in most test intervals. Fig. 5b of Rasmussen et al. (1993) suggests a good correlation between pneumatic and hydraulic permeabilities at the ALRS. A more detailed summary of this and other early work at the site can be found in Illman et al. (1998).

Single-hole pneumatic injection tests conducted at the ALRS by Rasmussen et al. (1990, 1993) were of relatively short duration and involved relatively long test intervals. Guzman et al. (1994, 1996) and Guzman and Neuman (1996) performed a much larger number of single-hole pneumatic injection tests of considerably longer duration over shorter injection intervals in six boreholes. A total of 184 borehole segments were tested by setting the packers 1 m apart. Additional tests were conducted in segments of lengths 0.5, 2.0 and 3.0 m in borehole Y2, and 2.0 m in borehole X2, bringing the total number of tests to over 270. The tests were conducted by maintaining a constant volumetric injection rate until air pressure in the test interval remained within 1 mm of Hg (133.33 Pa) for a period of 30 min. Pressure has reached stable values in most test

intervals, thus allowing the calculation of air permeability by means of steady-state formulae. The injection rate was then increased by a constant value and the procedure repeated. Three or more such incremental steps were conducted in each borehole segment while recording air injection rate, pressure, temperature and relative humidity. For each relatively stable period of injection rate and pressure, air permeability was estimated by treating the rock around each test interval as a uniform, isotropic continuum within which air flows as a single-phase under steady state, in a pressure field exhibiting prolate spheroidal symmetry. The results of these steady-state interpretations of single-hole air injection tests are listed in Guzman et al. (1996) and summarized in Guzman et al. (1994, 1996), Guzman and Neuman (1996) and Illman and Neuman (2000).

The work of Guzman et al. (1994, 1996) and Guzman and Neuman (1996) strongly suggests that air injection tests yield properties of the fracture system, which are relevant to both unsaturated and saturated conditions. In particular, numerical simulations by these authors show that, whereas the intrinsic permeability one determines from such tests is generally lower than the intrinsic permeability to water of fractures which surround the test interval, it nevertheless approaches the latter as the applied pressure goes up. This is so because capillary forces tend to draw water from fractures into the porous (matrix) blocks of rock between the fractures, thereby leaving the latter saturated primarily with air. Water saturation in the matrix blocks is therefore typically much higher than that within the fractures, making it relatively difficult for air to flow through such blocks. It follows that, during a pneumatic injection test, the air moves primarily through fractures (most of which contain relatively little water) and the test therefore yields flow and transport parameters which are only slightly below the intrinsic properties of these largely air-filled fractures.

Spatially distributed log air permeability data obtained from a steady-state interpretation of the 184 single-hole tests in 1 m borehole intervals were subjected to geostatistical analysis by Chen et al. (2000). The authors determined that these data could be viewed as a sample from a random field, which lacks a unique variance or correlation scale. Instead, the field constitutes a random fractal characterized by a large variance and a wide range of spatial correlation scales, both theoretically infinite. Using the geostatistical method of kriging, Chen et al. were able to estimate the way that log permeability varies in three-dimensional space between and around the boreholes. Their estimate is based on an augmented database of 227 values including the original 184 values corresponding to 1 m long test intervals, and 43 values obtained earlier by Rasmussen et al. (1990, 1993) from single-hole tests in 3 m intervals within boreholes X1, X3, Y1, Z1 and Z3, which have not been tested by Guzman et al. (1994, 1996).

Illman and Neuman (2000) used type-curves to interpret over 40 transient pressure data from the single-hole air injection tests previously conducted at the ALRS by Guzman et al. (1994, 1996) and Guzman and Neuman (1996). Their analyses provided information about air permeability, skin factor and dimensionality of the flow regime on a nominal scale of 1 m in the immediate vicinity of each test interval. The authors' transient air permeabilities agree well with previously determined steady-state values.

Most recently, Vesselinov and Neuman (2001) used a numerical inverse method to interpret simultaneously four sets of multi-rate injection and recovery data. Their model represents faithfully the three-dimensional geometry of boreholes at the site, and accounts directly for air storage and conductance properties by treating them as high-permeability and high-porosity cylinders of finite length and radius. It solves the airflow equations in their original non-linear form and yields information about air permeability, air-filled porosity and dimensionless borehole storage coefficient. Some of this is difficult to accomplish with analytical type-curves. Air permeability values obtained by their inverse method agree well with those obtained by steady-state and type-curve analyses.

4. Cross-hole pneumatic injection tests

Core and single-hole measurements, conducted over short segments of a borehole, provide information only about a small volume of rock in the immediate vicinity of each measurement interval. Available data from the ALRS indicate that rock

properties, measured on such small scales, vary erratically in space in a manner that renders the rock randomly heterogeneous. Chen et al. (2000) have conducted geostatistical analyses of several such variables. We show in Fig. 3, a three-dimensional representation of kriged log permeabilities obtained by them on the basis of single-hole pneumatic tests in borehole intervals of lengths 1 and 3 m. This smoothed image of spatial variability, together with other site information (primarily observed single-hole test behavior, borehole televiewer images, and core data relating to fracture distributions and matrix pneumatic and hydraulic properties), served as a guide in our design of cross-hole pneumatic injection tests at the ALRS. The purpose of these tests was to determine the bulk pneumatic properties of larger rock volumes between boreholes at the site, and the degree to which fractures are pneumatically interconnected. We conducted 44 cross-hole interference tests between 16 boreholes, six of which have been previously subjected to single-hole testing. The tests consisted of injecting air into an isolated interval within one borehole while monitoring pressure responses in isolated intervals within this and all other boreholes. Details concerning our tests, equipment and test procedure can be found in Illman et al. (1998).

The tests were performed using modular straddle packer systems that were easily adapted to various test configurations and allowed rapid replacement of failed components, modification of the number of packers, and adjustment of distances between them in

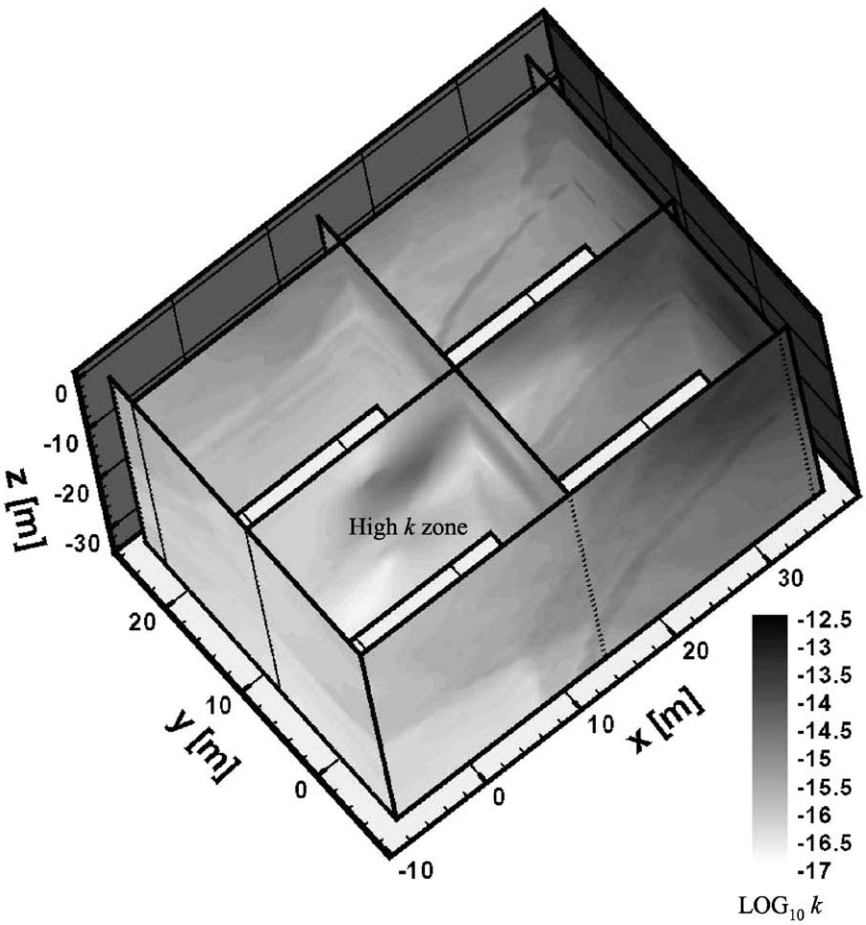

Fig. 3. Three-dimensional representation of kriged log k (adapted from Illman et al. (1998)).

both the injection and monitoring boreholes. The main injection string consisted of three packers, one near the soil surface to isolate the borehole from the atmosphere, and two to enclose the injection interval. The air-filled volume of the injection interval was made relatively small so as to minimize borehole storage effects. Intervals with a single packer near the soil surface (of which we had six) are identified below by borehole designation; for example V1, X1 and W1. Where a modular system separates a borehole into three isolated intervals, we append to the borehole designation a suffix U, M or B to identify the upper, middle or bottom interval, respectively; for example V3U, V3M and V3B. Where a modular system separates a borehole into four isolated intervals, we append to the borehole designation a suffix U, M, L or B to identify the upper, middle, lower or bottom interval, respectively; for example Z2U, Z2M, Z2L, and Z2B.

A typical cross-hole test consisted of packer inflation, a period of pressure recovery, air injection and another period of pressure recovery. Our system allowed rapid release of packer inflation pressure when the corresponding recovery was slow, but this feature was never activated even though recovery had sometimes taken several hours. Once packer inflation pressure had dissipated in all (monitoring and injection) intervals, air injection at a constant flow rate began. It generally continued for several days until pressure in most monitoring intervals appeared to have stabilized. In some tests, injection pressure was allowed to dissipate until ambient conditions have been recovered. In other tests, air injection continued at incremental flow rates, each lasting until the corresponding pressure had stabilized, before the system was allowed to recover.

5. Previous analyses of transient cross-hole test data

Illman and Neuman (2001) used type-curves to interpret the results of one cross-hole test, labeled PP4, by treating the fractured rock as a uniform isotropic continuum. The type-curves they used have been modified after Hsieh and Neuman (1985) to consider single-phase airflow and extended to consider the effects of storage and skin in monitoring intervals. Cross-hole type-curves of pressure derivatives and recovery were included for improved pneumatic characterization of the site. Each record yielded an equivalent directional air permeability and air-filled porosity for fractures that connect the corresponding monitoring and injection intervals, representing rock volumes with length-scales ranging from meters to a few tens of meters. Both parameters were found to vary considerably from one monitoring interval to another, reflecting the non-uniform nature of pneumatic rock properties at the ALRS. The geometric mean of these equivalent permeabilities exceeded by a factor of 50 that was obtained earlier by Guzman et al. (1996) from single-hole pneumatic injection tests, on a nominal scale of 1–3 m.

Based on these and related studies conducted at the site by various University of Arizona researchers, Illman and Neuman (2001) concluded that the pneumatic pressure behavior of unsaturated fractured tuffs at the ALRS can be described quite accurately by means of linearized single-phase airflow equations; this behavior can be interpreted by treating the rock as a continuum on scales ranging from meters to tens of meters; the continuum is representative primarily of interconnected fractures; as these fractures are filled primarily with air, their pneumatic permeabilities and porosities are close to the bulk intrinsic properties of fractures at the site; these intrinsic properties vary randomly with location and direction across the ALRS; and permeability depends strongly on the scale at which it is determined. Both the single-hole and cross-hole test results have proven to be virtually free of skin effect (Illman and Neuman, 2000, 2001), implying that they represent rock conditions unperturbed by the presence of boreholes.

Type-curve methods provide a relatively simple, fast and reliable way to interpret the results of pressure interference tests between boreholes in porous and fractured geologic media. Because type-curves are usually based on analytical solutions of the corresponding flow equations, they typically treat the medium as being composed of one, or very few, uniform constituents such as aquifers, aquitards, faults, dykes and/or fractures. For this

reason, they yield equivalent properties of the medium (permeability, specific storage or porosity) on scales comparable to distances between an injection or pumping well that generates a pressure signal, and monitoring wells in which pressure responses to this signal are observed. Type-curve methods cannot provide detailed information about the spatial variability of medium properties on scales smaller than these distances. To obtain such information, it was suggested by Neuman (1987) that the rock is treated as a stochastic continuum, and its properties estimated by the simultaneous numerical inversion of multiple pressure signals, sent across the rock from various boreholes in various directions. Neuman's (1987) suggestion arose in the context of hydraulic cross-hole tests conducted by Hsieh et al. (1985) in a saturated crystalline rock mass near Oracle, Arizona, which, however, have not been interpreted in this way. Since the idea is akin to geophysical characterization methods, such as seismic and electromagnetic tomography, Neuman termed his proposed approach 'hydraulic tomography.'

Our pneumatic cross-hole tests were designed so as to allow using them for pneumatic tomography of fractured rock at the ALRS. This was accomplished by Vesselinov et al. (2001a,b) by using a three-dimensional numerical inverse model to interpret several cross-hole pneumatic tests at the ALRS. The authors analyzed pneumatic cross-hole test data by treating the rock as being either (a) spatially uniform or (b) a random fractal characterized by a power variogram. The first approach yielded a series of equivalent log air permeability (and log air-filled porosity) estimates analogous to the type-curve estimates of Illman and Neuman (2001). The second approach yielded a high-resolution estimate of how air permeability and air-filled porosity, defined on grid blocks having a length-scale of 1 m, vary spatially throughout the tested rock volume. The approach entailed geostatistical inversion of the cross-hole test data to yield estimates at 'pilot points'. Projecting these estimates onto the simulation domain by kriging yielded a tomographic image of rock heterogeneity. Five cross-hole tests (PP4–PP8) have been analyzed by treating the rock to be spatially uniform and three tests (PP4–PP6) by treating the rock as a random fractal.

6. Steady-state analysis of cross-hole test data

Recently, we have used a steady-state approach to analyze data from a larger set of cross-hole tests than had been interpreted previously by transient methods. Our steady-state analysis was conducted on tests deemed successful in that (1) they did not suffer from significant equipment failure and (2) their flow conditions were relatively well controlled and stable. These tests are listed in Table 1, which identifies them by name, injection borehole, injection interval measured along the borehole relative to the lower lip of the casing, injection flow rate, and permeability computed on the basis of pressure within the injection interval by means of a steady-state formula previously used for single-hole test interpretation by Guzman et al. (1996).

In Table 1, PL designates point-injection/line-monitoring tests in which air was injected into a 2 m section in one borehole while pressure was recorded along the entire length of each monitoring borehole. We analyze data from six such tests (PL3, PL4, PL8, PL9, PL10, PL15) none of which have been previously analyzed. In all these tests, air was injected into various intervals within borehole Y2 that are surrounded by low to moderately permeable rock. PP designates point-injection/point-monitoring tests in which both the injection and the monitoring intervals were short enough to be regarded, for purposes of

Table 1
Test name, name of injection borehole, upper and lower extent of injection interval measured along borehole from lower lip of casing, injection flow rate (Q), and injection interval permeability computed by means of a steady-state formula given in Guzman et al. (1996)

Test name	Injection borehole	Injection interval (m)	Q (slpm)	k (m^2)
PL3	Y2	15.0–17.0	20	4.10×10^{-14}
PL4	Y2	21.0–23.0	1	2.64×10^{-15}
PL8	Y2	18.0–20.0	1	3.03×10^{-15}
PL9	Y2	26.0–28.0	1	1.08×10^{-15}
PL10	Y2	23.0–25.0	1	1.51×10^{-15}
PL15	Y2	21.0–23.0	1	2.29×10^{-15}
PP4	Y2	15.0–17.0	50.0	5.55×10^{-14}
PP5	X2	18.5–20.7	5.0	5.13×10^{-15}
PP6	Z3	15.9–17.9	5.0	1.06×10^{-14}
PP7	W3	19.2–20.4	5.0	2.25×10^{-14}
PP8	Y2	15.0–17.0	50.0	5.37×10^{-14}

analysis, as points. We analyze data from five such tests (PP4–PP8) which were previously subjected to transient analyses by Illman and Neuman (2001) (PP4) and Vesselinov et al. (2001a,b) (PP4–PP8). Their transient analysis was made possible by the relatively high permeability of the injection intervals (Table 1), which in turn has allowed relatively distinct transient pressure signals to develop in monitoring intervals.

Fig. 4 shows arithmetic plots of pressure responses in monitoring intervals V1, V2, and V3 (of lengths 29.53, 24.25 and 26.48 m, respectively) during cross-hole test PL15. Pressure in the monitoring intervals is seen to reach a stable value after 10,000 s following the start of injection. A barometric pressure record is included to help explain why we have analyzed data from V1 and V2 but not from V3, in which the former exceed the pressure signal.

Fig. 5 shows arithmetic plots of pressure responses in monitoring intervals W2AU, W2AM, W2AL, and W2AB (of lengths 6.66, 1.54, 2.07 and 3.96 m, respectively) during cross-hole test PP4. Pressure is seen to have reached stable values after 50,000 s following the start of injection. The signal-to-noise ratio is relatively large in all four monitoring intervals.

A visual examination of all pressure records reveals that many of them attain near-stable values at sufficiently large time and should, therefore, be amenable to steady-state analysis. We consider the arithmetic average of such late data to represent steady-state pressure. Our criterion for what constitutes steady-state is somewhat more lax than that adopted by Guzman et al. (1996) for their single-hole test interpretations.

Table 2 lists coordinates of the centroid of each test interval (with origin at the center of the injection interval), its length B, radial distances R from the centroid of the monitoring interval to that of the injection interval, angle θ in radians between a unit vector $\mathbf{e}$ pointing from the centroid of the injection interval toward the centroid of the monitoring interval and a unit vector $\mathbf{e}_b$ parallel to the monitoring interval, the geometric parameters $\beta_1 = 2R/B$ and $\beta_2 = \cos\theta$, and the pressure increment that we take to represent

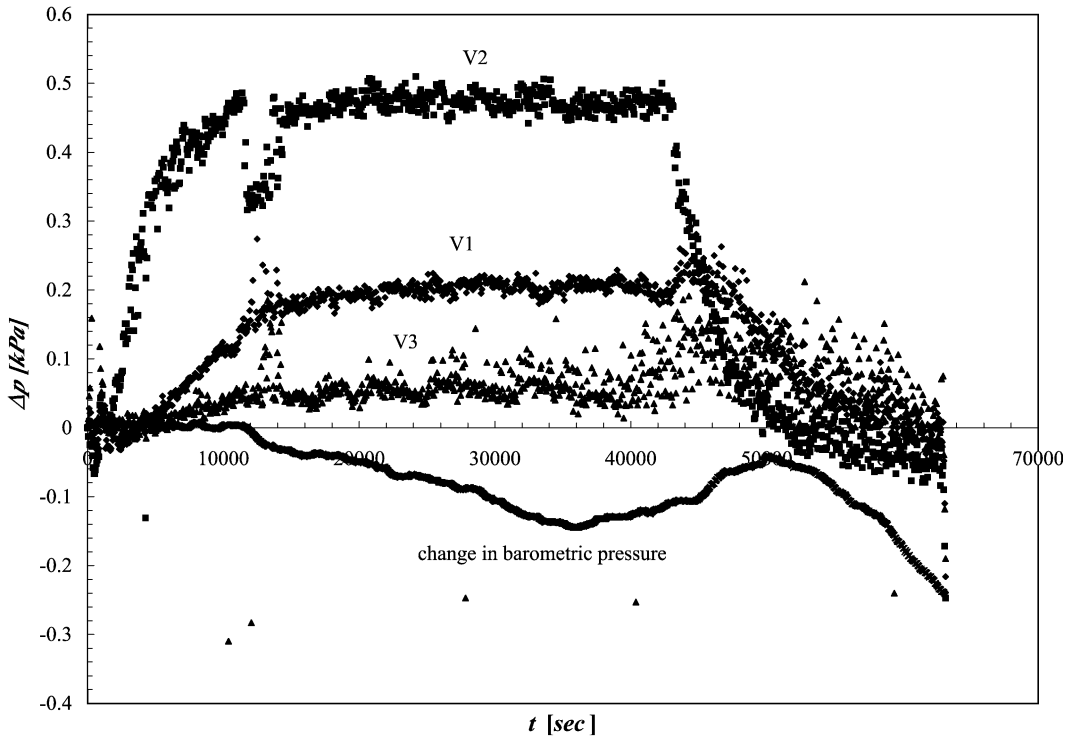

Fig. 4. Pressure in monitoring intervals V1, V2, and V3 during cross-hole test PL15.

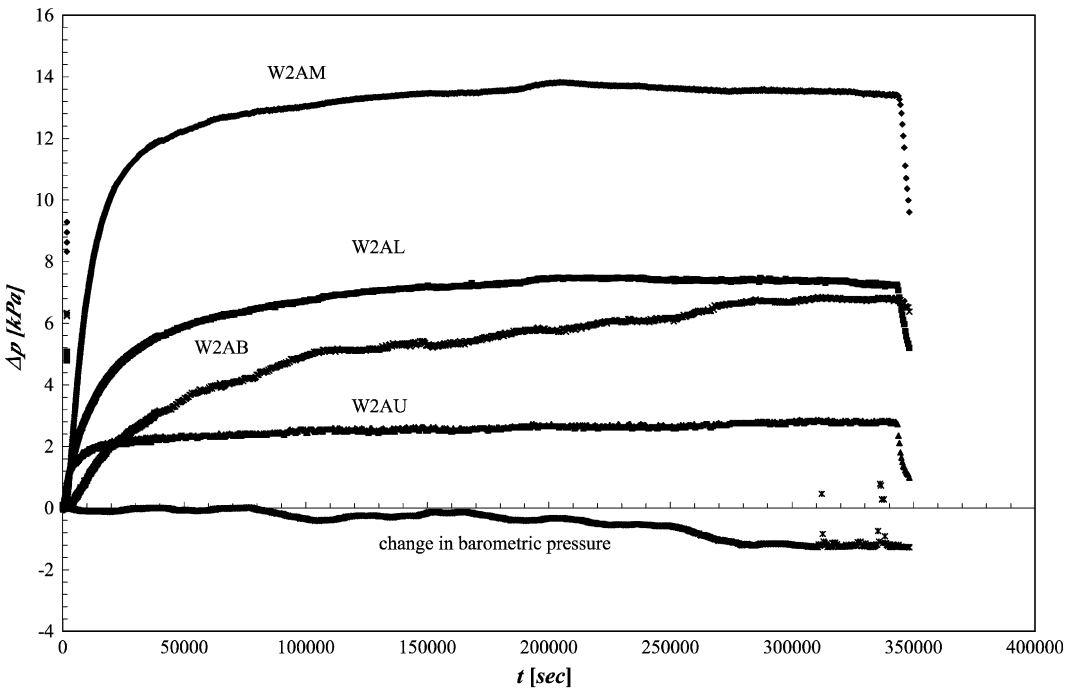

Fig. 5. Pressure in monitoring intervals W2AU, W2AM, W2AL, and W2AB during cross-hole test PP4.

steady-state in the interval. Also included in Table 2 are permeabilities k calculated by the steady-state formula

$$k=\frac{Q\mu}{4\pi R\bar{p}}\frac{\beta_1}{2}\ln\frac{(\beta_1^2+2\beta_1\beta_2+1)^{1/2}+\beta_1\beta_2+1}{(\beta_1^2-2\beta_1\beta_2+1)^{1/2}+\beta_1\beta_2-1} \quad (1)$$

where Q is injection rate, μ is dynamic viscosity and $\bar{p}$ is the average steady-state pressure increment. The formula is an isotropic version of one developed by Hsieh and Neuman (1985) for saturated flow in a uniform, anisotropic porous medium. It treats the injection interval as a point source and the monitoring intervals as lines of variable lengths. We take permeability to be a scalar because we do not expect to capture the heterogeneity pattern in Fig. 3 by means of an equivalent anisotropic model any better than we do by means of an equivalent isotropic model.

The equations that describe airflow in partially saturated porous media are non-linear due to the compressible nature of air, its capillary interaction with water, and non-Darcian behavior at high Reynolds numbers. A complete description of air–water interaction requires two systems of coupled partial differential equations, one for each phase. The development of corresponding analytical formulae requires that two-phase flow is approximated as single-phase airflow and that water is treated as immobile. The airflow equation must additionally be linearized to allow solving it either in terms of pressure, p, as is customary for liquids or in terms of pressure-squared, p^2, as is more common for gases. Details to the theoretical development are provided in Illman and Neuman (2001). Illman and Neuman (2000) have shown that interpreting single-hole pneumatic injection tests at the ALRS by means of p^2-based and p-based type-curves leads to similar results. Illman and Neuman (2001) have shown that the same holds true for cross-hole tests and, therefore, adopt the simpler p-based representation, as we do here.

Enhanced permeability due to slip flow (the Klinkenberg effect) was shown by Guzman et al. (1994, 1996) and Guzman and Neuman (1996) to be of little relevance for the interpretation of air injection tests at the ALRS. This is so because most of these tests ‘see’ fractures, which have

Table 2
Geometric parameters, steady-state pressure and permeability associated with each cross-hole test interval

	x (m)	y (m)	z (m)	B (m)	R (m)	θ (rad)	β_1	β_2	$\bar{p}$ (kPa)	k (m^2)
PL3										
V1	−7.17	1.64	−6.84	29.53	10.04	0.82	0.68	0.68	0.89	4.98×10^{-14}
V2	−4.18	1.64	−4.20	24.25	6.15	0.82	0.51	0.68	4.38	1.51×10^{-14}
V3	−1.18	1.64	−5.31	26.48	5.68	0.36	0.43	0.93	17.71	5.11×10^{-15}
W1	−3.57	0.31	4.91	11.85	6.07	0.92	1.03	0.61	3.90	1.96×10^{-14}
W2A	−3.18	4.16	−0.20	26.14	5.24	1.01	0.40	0.53	6.66	9.83×10^{-15}
W3	−3.38	7.88	−7.14	45.93	11.15	1.52	0.49	0.05	1.82	1.69×10^{-14}
X1	−6.01	4.84	4.03	14.44	8.70	1.41	1.21	0.16	3.01	1.68×10^{-14}
X2	−0.94	4.83	−1.05	28.61	5.03	1.29	0.35	0.28	3.75	1.61×10^{-14}
Y1	−5.73	−0.12	4.38	13.19	7.21	1.44	1.09	0.13	2.87	2.09×10^{-14}
Y2M	0.00	0.00	0.00	2.00					17.87	4.10×10^{-14}
Y3	4.10	0.15	−5.90	40.90	7.18	1.39	0.35	0.18	0.19	2.16×10^{-13}
Z2	14.13	−5.17	−1.02	27.50	15.08	0.78	1.10	0.71	0.10	3.31×10^{-13}
PL4										
V1	−2.93	1.64	−2.59	29.53	4.24	0.91	0.29	0.61	0.09	3.87×10^{-14}
V2	0.06	1.64	0.05	24.25	1.65	1.54	0.14	0.03	0.09	5.81×10^{-14}
W2A	1.07	4.16	4.04	26.14	5.89	0.18	0.45	0.98	0.97	5.85×10^{-15}
Y2M	0.00	0.00	0.00	2.00					38.83	2.64×10^{-15}
PL8										
V3	0.94	1.64	−3.19	26.48	3.71	0.54	0.28	0.86	0.83	5.71×10^{-15}
W2A	−1.05	4.16	1.92	26.14	4.70	0.42	0.36	0.91	0.69	6.84×10^{-15}
Y2M	0.00	0.00	0.00	2.00					33.23	3.03×10^{-15}
PL9										
V1	0.61	1.64	0.94	29.53	1.99	1.08	0.13	0.47	1.09	4.20×10^{-15}
Y2M	0.00	0.00	0.00	2.00					110.37	1.08×10^{-15}
PL10										
V1	−1.51	1.64	−1.18	29.53	2.53	1.08	0.17	0.47	0.44	9.56×10^{-15}
V3	4.48	1.64	0.34	26.48	4.78	1.50	0.36	0.07	0.15	2.05×10^{-14}
W3	2.28	7.88	−1.48	45.93	8.33	1.00	0.36	0.54	0.03	5.98×10^{-14}
Y2M	0.00	0.00	0.00	2.00					74.20	1.51×10^{-15}
PL15										
V1	−2.93	1.64	−2.59	29.53	4.24	0.91	0.29	0.61	0.18	1.98×10^{-14}
V2	0.06	1.64	0.05	24.25	1.65	1.54	0.14	0.03	0.49	1.08×10^{-14}
W2AM	1.07	1.16	1.03	1.54	1.88	0.60	2.45	0.82	1.84	7.12×10^{-15}
W2AL	1.07	−0.82	−0.94	2.07	1.64	0.71	1.58	0.76	1.33	1.14×10^{-14}
Y2M	0.00	0.00	0.00	2.00					45.51	2.29×10^{-15}
PP4										
V1	−7.17	1.64	−6.84	29.53	10.04	0.82	0.68	0.68	8.03	1.38×10^{-14}
V2M	−4.18	1.64	3.92	2.03	5.96	0.85	5.87	0.66	9.34	2.16×10^{-14}
V3U	−1.18	1.64	6.08	9.56	6.41	0.32	1.34	0.95	5.57	4.01×10^{-14}
V3M	−1.18	1.64	−0.32	0.50	2.05	1.41	8.19	0.16	48.07	1.22×10^{-14}
V3B	−1.18	1.64	−9.50	18.11	9.71	0.21	1.07	0.98	23.17	7.71×10^{-15}
W1	−3.57	0.31	4.91	11.85	6.07	0.92	1.03	0.61	8.74	2.19×10^{-14}
W2AU	−3.18	4.75	0.39	6.66	5.73	0.88	1.72	0.63	2.80	7.51×10^{-14}
W2AM	−3.18	1.15	−3.21	1.54	4.66	1.25	6.05	0.31	13.45	1.91×10^{-14}
W2AL	−3.18	−0.81	−5.18	2.07	6.13	0.81	5.92	0.69	7.27	2.70×10^{-14}
W2AB	−3.18	−3.68	−8.05	3.96	9.40	0.49	4.75	0.88	6.78	1.90×10^{-14}
W3U	−3.38	16.50	1.49	6.81	16.91	0.72	4.97	0.75	4.30	1.66×10^{-14}

Table 2 (*continued*)

	x (m)	y (m)	z (m)	B (m)	R (m)	θ (rad)	β_1	β_2	$\bar{p}$ (kPa)	k (m^2)
W3M	−3.38	12.93	−2.09	1.23	13.53	0.97	21.99	0.57	4.29	2.07×10^{-14}
X1	−6.01	4.84	4.03	14.44	8.70	1.41	1.21	0.16	6.30	2.00×10^{-14}
X2U	2.55	4.83	2.44	8.16	5.98	0.94	1.47	0.59	8.51	2.33×10^{-14}
X2M	−1.83	4.83	−1.94	2.20	5.52	1.07	5.02	0.48	17.33	1.25×10^{-14}
X2B	−7.89	4.83	−8.01	12.94	12.24	0.41	1.89	0.92	6.94	1.52×10^{-14}
Y1M	−2.83	−0.12	7.28	1.83	7.81	1.16	8.54	0.40	6.84	2.24×10^{-14}
Y2U	3.96	0.00	3.96	7.12	5.60	1.56	1.57	0.01	16.78	1.20×10^{-14}
Y2M	0.00	0.00	0.00	2.00					106.79	5.55×10^{-14}
Y2B	−5.99	0.00	−5.99	12.94	8.47	1.56	1.31	0.01	21.38	6.11×10^{-15}
Y3U	14.83	0.15	4.84	7.46	15.60	0.47	4.18	0.89	0.50	1.55×10^{-13}
Y3M	10.73	0.15	0.74	2.03	10.76	0.72	10.63	0.75	0.61	1.84×10^{-13}
Y3B	−0.54	0.15	−10.53	27.78	10.55	0.73	0.76	0.74	2.53	4.47×10^{-14}
Z1	18.87	−5.20	3.83	13.04	19.95	1.01	3.06	0.53	0.11	5.31×10^{-13}
Z2U	10.52	−5.17	2.60	8.06	12.00	1.09	2.98	0.47	0.68	1.46×10^{-13}
Z2M	14.80	−5.17	−1.69	2.00	15.77	0.74	15.77	0.74	0.27	2.85×10^{-13}
Z2L	16.94	−5.17	−3.83	2.01	18.12	0.63	18.03	0.81	0.13	5.14×10^{-13}
Z2B	21.12	−5.17	−8.00	7.74	23.17	0.48	5.99	0.89	0.13	4.17×10^{-13}
Z3U	−0.30	−5.20	3.80	6.81	6.45	1.10	1.89	0.45	6.26	2.91×10^{-14}
Z3M	3.54	−5.20	−0.03	2.00	6.29	1.16	6.29	0.40	6.63	2.87×10^{-14}
Z3B	14.37	−5.20	−10.86	25.98	18.75	0.31	1.44	0.95	0.16	4.55×10^{-13}
PP5										
V1	−5.34	−3.19	−4.90	29.53	7.92	0.90	0.54	0.62	0.75	1.69×10^{-14}
V2M	−2.35	−3.19	5.86	2.03	7.08	0.59	6.97	0.83	0.40	4.21×10^{-14}
V3U	0.65	−3.19	8.02	9.56	8.65	0.39	1.81	0.93	0.38	4.02×10^{-14}
V3M	0.65	−3.19	1.62	0.50	3.63	1.11	14.53	0.45	1.40	2.36×10^{-14}
V3B	0.65	−3.19	−7.56	18.11	8.23	0.41	0.91	0.92	13.49	1.37×10^{-15}
W1	−1.74	−4.52	6.85	11.85	8.39	1.37	1.42	0.20	0.44	3.07×10^{-14}
W2AU	−1.35	−0.08	2.33	6.66	2.69	0.94	0.81	0.59	0.24	1.73×10^{-13}
W2AM	−1.35	−3.68	−1.27	1.54	4.12	0.56	5.35	0.85	4.67	6.28×10^{-15}
W2AL	−1.35	−5.65	−3.24	2.07	6.65	0.33	6.42	0.95	0.61	2.97×10^{-14}
W3U	−1.55	11.67	3.43	6.81	12.26	0.51	3.60	0.87	0.07	1.42×10^{-13}
W3M	−1.55	8.10	−0.15	1.23	8.25	0.82	13.41	0.68	0.66	2.21×10^{-14}
X1	−4.18	0.01	5.97	14.44	7.29	1.40	1.01	0.17	0.35	4.20×10^{-14}
X2U	4.38	0.00	4.38	8.16	6.19	1.56	1.52	0.01	0.98	1.86×10^{-14}
X2M	0.00	0.00	0.00	2.20					117.60	5.13×10^{-15}
X2B	−6.07	0.00	−6.07	12.94	8.58	1.56	1.33	0.01	2.55	5.06×10^{-15}
Y2U	5.79	−4.83	5.90	7.12	9.57	0.53	2.69	0.86	0.77	1.68×10^{-14}
Y2M	1.83	−4.83	1.94	2.00	5.52	1.07	5.52	0.48	1.51	1.44×10^{-14}
Y2B	−4.16	−4.83	−4.05	12.94	7.55	0.69	1.17	0.77	5.55	3.01×10^{-15}
Y3B	1.29	−4.68	−8.59	27.78	9.87	1.02	0.71	0.52	0.39	2.74×10^{-14}
Z2U	12.34	−10.00	4.54	8.06	16.52	1.23	4.10	0.33	0.03	2.89×10^{-13}
Z3U	1.53	−10.03	5.74	6.81	11.66	1.31	3.42	0.26	0.08	1.21×10^{-13}
Z3M	5.37	−10.03	1.91	2.00	11.54	1.36	11.54	0.21	0.28	3.70×10^{-14}
PP6										
V1	−10.71	6.84	−6.81	29.53	14.42	1.08	0.98	0.47	0.53	1.44×10^{-14}
V2M	−7.72	6.84	3.95	2.03	11.05	1.20	10.88	0.36	0.54	2.00×10^{-14}
V3U	−4.72	6.84	6.11	9.56	10.32	0.94	2.16	0.59	0.65	1.79×10^{-14}
V3M	−4.72	6.84	−0.29	0.50	8.32	1.54	33.27	0.03	0.66	2.18×10^{-14}
V3B	−4.72	6.84	−9.47	18.11	12.60	0.72	1.39	0.75	0.47	2.12×10^{-14}
W1	−7.11	5.51	4.94	11.85	10.26	0.77	1.73	0.72	0.63	1.90×10^{-14}
W2AM	−6.72	6.35	−3.18	1.54	9.78	1.34	12.70	0.23	0.66	1.85×10^{-14}

(*continued on next page*)

Table 2 (*continued*)

	x (m)	y (m)	z (m)	B (m)	R (m)	θ (rad)	β_1	β_2	$\bar{p}$ (kPa)	k (m^2)
W2AL	−6.72	4.39	−5.15	2.07	9.53	1.51	9.21	0.06	0.77	1.62×10^{-14}
W2AB	−6.72	1.52	−8.01	3.96	10.57	1.12	5.34	0.43	0.63	1.80×10^{-14}
X1	−9.55	10.04	4.06	14.44	14.44	1.30	2.00	0.27	0.47	1.72×10^{-14}
X2U	−0.99	10.03	2.47	8.16	10.38	1.47	2.55	0.10	0.31	3.67×10^{-14}
X2M	−5.37	10.03	−1.91	2.20	11.54	1.11	10.49	0.45	0.50	2.07×10^{-14}
X2B	−11.43	10.03	−7.97	12.94	17.17	0.65	2.66	0.80	0.34	2.13×10^{-14}
Y2U	0.42	5.20	3.99	7.12	6.57	1.08	1.85	0.47	0.64	2.81×10^{-14}
Y2M	−3.54	5.20	0.03	2.00	6.29	1.17	6.29	0.39	0.71	2.70×10^{-14}
Y2B	−9.53	5.20	−5.96	12.94	12.38	0.49	1.91	0.88	0.54	1.91×10^{-14}
Y3B	−4.08	5.35	−10.50	27.78	12.47	0.60	0.90	0.83	0.23	4.65×10^{-14}
Z3U	−3.84	0.00	3.84	6.81	5.43	1.56	1.59	0.01	3.98	5.25×10^{-15}
Z3M	0.00	0.00	0.00	2.00					49.69	1.06×10^{-14}
PP7										
V1	−3.79	−11.29	−4.75	29.53	12.82	1.19	0.87	0.37	0.61	1.35×10^{-14}
V2M	−0.80	−11.29	6.01	2.03	12.81	1.08	12.62	0.47	0.63	1.50×10^{-14}
V3U	2.20	−11.29	8.16	9.56	14.10	0.95	2.95	0.58	0.48	1.76×10^{-14}
V3M	2.20	−11.29	1.76	0.50	11.63	1.42	46.53	0.15	0.62	1.67×10^{-14}
V3B	2.20	−11.29	−7.41	18.11	13.68	1.00	1.51	0.54	0.50	1.74×10^{-14}
W1	−0.19	−12.62	6.99	11.85	14.43	1.29	2.43	0.28	0.65	1.25×10^{-14}
W2AM	0.20	−11.78	−1.12	1.54	11.83	0.69	15.36	0.77	0.58	1.75×10^{-14}
W2AL	0.20	−13.75	−3.09	2.07	14.09	0.56	13.61	0.85	0.37	2.30×10^{-14}
W3U	0.00	3.57	3.57	6.81	5.05	1.56	1.48	0.01	7.76	2.87×10^{-15}
W3M	0.00	0.00	0.00	1.23					21.48	2.25×10^{-14}
X1	−2.63	−8.09	6.12	14.44	10.48	1.33	1.45	0.24	0.81	1.34×10^{-14}
X2U	5.93	−8.10	4.52	8.16	11.01	0.83	2.70	0.67	0.68	1.63×10^{-14}
X2M	1.55	−8.10	0.15	2.20	8.25	1.42	7.50	0.15	0.98	1.48×10^{-14}
X2B	−4.52	−8.10	−5.92	12.94	11.00	0.84	1.70	0.67	0.97	1.13×10^{-14}
Y2M	3.38	−12.93	2.09	2.00	13.53	1.28	13.53	0.29	0.63	1.41×10^{-14}
Y3B	2.84	−12.78	−8.45	27.78	15.58	1.31	1.12	0.25	0.34	2.08×10^{-14}
PP8										
V1	−7.17	1.64	−6.84	29.53	10.04	0.82	0.68	0.68	7.40	1.51×10^{-14}
V2M	−4.18	1.64	3.92	2.03	5.96	0.85	5.87	0.66	9.16	2.21×10^{-14}
V3U	−1.18	1.64	6.08	9.56	6.41	0.32	1.34	0.95	11.57	1.94×10^{-14}
V3M	−1.18	1.64	−0.32	0.50	2.05	1.41	8.19	0.16	47.32	1.24×10^{-14}
V3B	−1.18	1.64	−9.50	18.11	9.71	0.21	1.07	0.98	22.27	8.06×10^{-15}
W1	−3.57	0.31	4.91	11.85	6.07	0.92	1.03	0.61	8.79	2.18×10^{-14}
W2AU	−3.18	4.75	0.39	6.66	5.73	0.88	1.72	0.63	2.49	8.47×10^{-14}
W2AM	−3.18	1.15	−3.21	1.54	4.66	1.25	6.05	0.31	12.77	2.02×10^{-14}
W2AL	−3.18	−0.81	−5.18	2.07	6.13	0.81	5.92	0.69	6.37	3.09×10^{-14}
W2AB	−3.18	−3.68	−8.05	3.96	9.40	0.49	4.75	0.88	4.03	3.21×10^{-14}
W3U	−3.38	16.50	1.49	6.81	16.91	0.72	4.97	0.75	2.70	2.66×10^{-14}
W3M	−3.38	12.93	−2.09	1.23	13.53	0.97	21.99	0.57	4.10	2.17×10^{-14}
X1	−6.01	4.84	4.03	14.44	8.70	1.41	1.21	0.16	6.47	1.96×10^{-14}
X2U	2.55	4.83	2.44	8.16	5.98	0.94	1.47	0.59	9.06	2.20×10^{-14}
X2M	−1.83	4.83	−1.94	2.20	5.52	1.07	5.02	0.48	16.81	1.30×10^{-14}
X2B	−7.89	4.83	−8.01	12.94	12.24	0.41	1.89	0.92	6.59	1.61×10^{-14}
Y1M	−2.83	−0.12	7.28	1.83	7.81	1.16	8.54	0.40	6.80	2.27×10^{-14}
Y2U	3.96	0.00	3.96	7.12	5.60	1.56	1.57	0.01	15.02	1.35×10^{-14}
Y2M	0.00	0.00	0.00	2.00					111.71	5.37×10^{-14}
Y2B	−5.99	0.00	−5.99	12.94	8.47	1.56	1.31	0.01	19.02	6.90×10^{-15}
Y3U	11.29	0.15	1.30	7.46	11.37	0.67	3.05	0.78	0.68	1.58×10^{-13}
Y3M	7.20	0.15	−2.79	2.03	7.72	1.16	7.63	0.40	1.53	1.02×10^{-13}

Table 2 (*continued*)

	x (m)	y (m)	z (m)	B (m)	R (m)	θ (rad)	β_1	β_2	$\bar{p}$ (kPa)	k (m^2)
Y3B	−2.31	0.15	−12.30	22.78	12.52	0.60	1.10	0.83	3.04	3.46×10^{-14}
Z1	18.87	−5.20	3.83	13.04	19.95	1.01	3.06	0.53	0.16	3.79×10^{-13}
Z2U	10.52	−5.17	2.60	8.06	12.00	1.09	2.98	0.47	0.70	1.42×10^{-13}
Z2M	14.80	−5.17	−1.69	2.00	15.77	0.74	15.77	0.74	0.34	2.25×10^{-13}
Z2L	16.94	−5.17	−3.83	2.01	18.12	0.63	18.03	0.81	0.17	3.89×10^{-13}
Z2B	21.12	−5.17	−8.00	7.74	23.17	0.48	5.99	0.89	0.14	3.71×10^{-13}

mean apertures that are considerably larger than the mean pore diameter of intact matrix at the site. For a more detailed explanation of the role that slip flow plays in pneumatic tests at the site the reader is referred to Appendix C in Illman (1999).

Guzman et al. (1994, 1996) and Guzman and Neuman (1996) also found that whereas inertial (non-linear, non-Darcian) behavior was limited to only a few test intervals intersected by highly permeable fractures, flow in most test intervals appeared to be Darcian. We (Illman and Neuman, 2001) expect inertial flow during cross-hole tests to be limited to the immediate vicinity of the injection interval and thus to have at most a minor impact on pressures recorded within monitoring intervals.

Table 2 lists results of steady-state analyses from 138 monitoring intervals during cross-hole tests PL3, PL4, PL8, PL9, PL10, PL15 and PP4–PP8. Data from 142 intervals were not amenable to steady-state interpretation because there was no identifiable signal. Our analysis of pressure data from any given monitoring interval assumes that the rock is pneumatically uniform and isotropic on the scale of the cross-hole test. However, data from different monitoring intervals are seen to yield different values of pneumatic parameters, thereby providing information about their spatial and directional dependence. The values of k can be viewed as bulk directional properties of the rock associated with given injection and monitoring intervals.

7. Statistical analysis of results

Results from test series PL and PP reflect different test conditions and are therefore examined separately. LOG_{10}-transformed k values from the PL series range from -14.38 (4.17×10^{-15} m^2) to -12.48 (3.31×10^{-13} m^2) with a mean of -13.74 (1.82×10^{-14} m^2), variance of 0.23, and coefficient of variation equal to -0.035. If we exclude $\log_{10}$-transformed k values from test PL3 (during which injection took place into an interval of relatively large permeability), the mean drops slightly to -13.87 (1.34×10^{-14} m^2) with a variance of 0.15 and coefficient of variation equal to -0.39.

LOG_{10}-transformed k values corresponding to PP tests range from -14.86 (1.38×10^{-15} m^2) to -12.28 (5.25×10^{-13} m^2) with a mean of -13.54 (2.88×10^{-14} m^2), variance of 0.26, and coefficient of variation equal to -0.037.

Fig. 6 depicts a histogram of $\log_{10}$-transformed pneumatic permeability, corresponding to all the tests listed in Table 2. Fig. 7 shows that $\log_{10}$-transformed permeabilities previously obtained for test PP4 by Illman and Neuman (2001) using transient type-curves correlate well with steady-state results obtained by us here for the same test. Fig. 8 compares numerical inverse results previously obtained by Vesselinov (2000) and Vesselinov et al. (2001a,b) for tests PP4–PP8 by treating the medium as a uniform continuum and our steady-state results for the same tests. The two differ somewhat from each other for reasons explained by Vesselinov et al.

8. Permeability scale effect

Previous analyses of single-hole and cross-hole pneumatic injection tests have pointed to a pronounced permeability scale effect at the ALRS (Illman and Neuman, 2001; Vesselinov et al.,

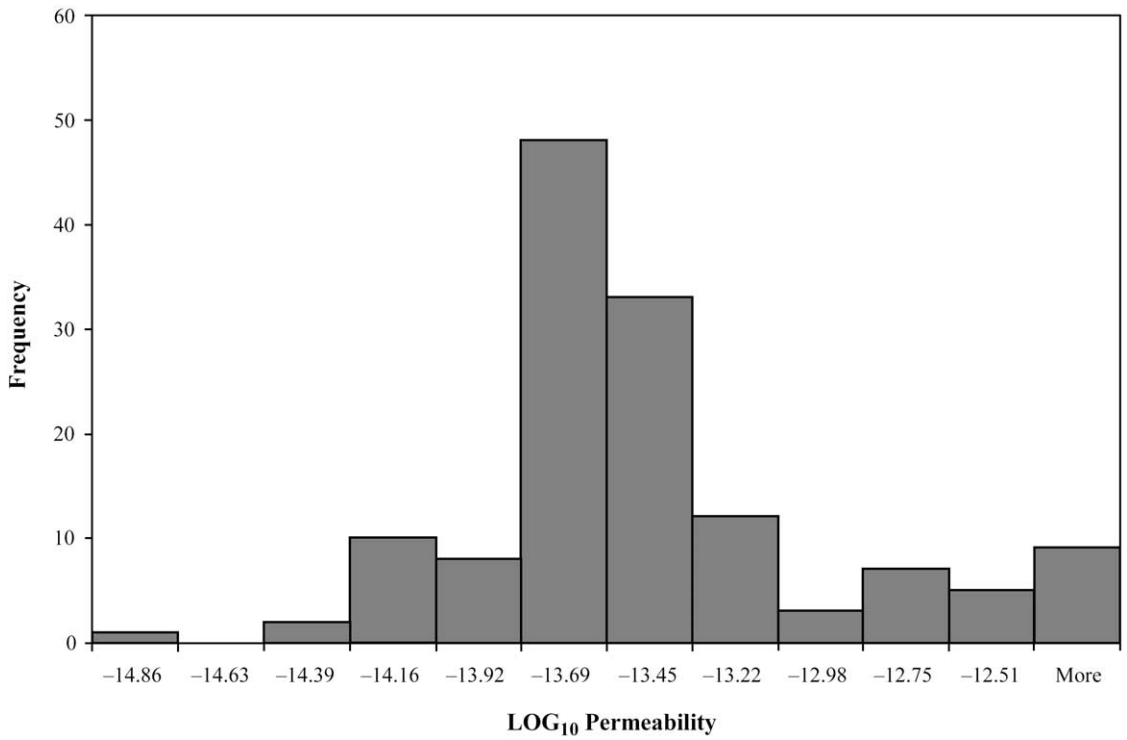

Fig. 6. Histogram of log-permeabilities estimated by the steady-state approach.

2001a,b; Hyun et al., 2002). The results of our steady-state cross-hole test analyses provide further support for this scale effect by significantly enlarging the corresponding database and eliminating any (previously plausible) suspicion that the cross-hole test data may be biased toward injection into intervals of relatively high permeability. The results of our steady-state analysis are based on numerous cross-hole tests in which injection took place into intervals of low to intermediate permeability. These results are included in Table 3, which clearly reveals a steep increase in the mean value of log permeability estimates with the scales of observation and/or resolution. The smallest scale, on the order of 1 m, corresponds to single-hole test results and to tomographic (kriged) inverse estimates based on the cross-hole tests. The largest scale, on the order of tens of meters, corresponds to cross-hole test results obtained analytically using our steady-state approach in this paper and type-curves, as well as numerical inverse estimates obtained upon treating the rock as being uniform. Mean values obtained by different methods at any given scale of estimation are generally comparable. Yet mean values obtained from cross-hole tests under the uniform rock assumption are consistently larger than those obtained by allowing pneumatic properties to vary spatially over distances of 1 m.

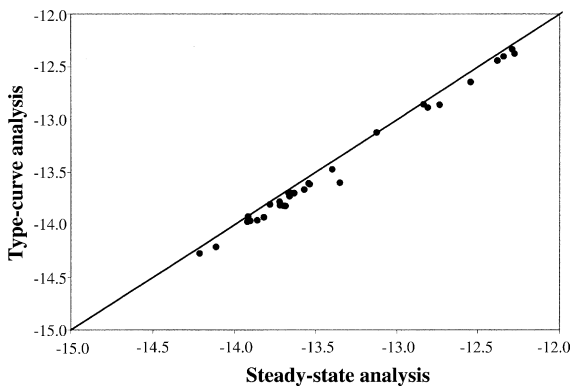

Fig. 7. Log-permeability estimated using the steady-state formula and the type-curve interpretation (Illman and Neuman, 2001) from PP4 test data.

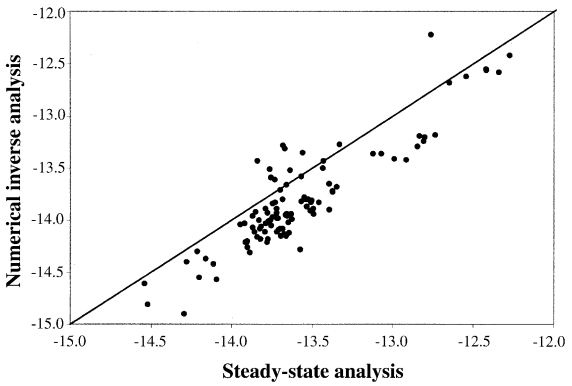

Fig. 8. Log-permeability estimated using the steady-state formula and the numerical inverse model (Vesselinov et al., 2001a,b) from PP4, PP5, PP6, PP7, and PP8 test data.

For example, the mean of steady-state log permeability estimates obtained from cross-hole tests PL3, 4, 8, 9, 10, 15 and PP4–8 when treating the rock as being spatially uniform (−13.57) exceeds the mean of the steady-state estimates from the single-hole tests (−15.22) by 1.65. This represents a 45-fold increase in the associated values of permeability. The mean of inverse log permeability estimates obtained from cross-hole tests PP4–PP6 when treating the rock as being spatially uniform (−13.70) exceeds the mean of simultaneous tomographic estimates from the same three tests (−15.69) by 1.99. This represents a 98-fold increase in the associated values of permeability. The mean of log permeability estimates obtained by inverting cross-hole test PP4 when treating the rock as being uniform (−13.57) exceeds the average of mean tomographic estimates obtained from this test using 64 pilot points (−14.77) by 1.20. This represents an increase in the associated values of permeability by a factor of about 16. The average of all uniform inverse mean estimates in Table 3 (−13.64) exceeds that of all tomographic mean estimates (−15.23) by 1.59, which corresponds to an increase in the associated value of permeability by a factor of 39.

The observed permeability scale effect at the ALRS is clearly unrelated to the method of testing: there is consistency between single-hole and cross-hole test results corresponding to a wide range of injection rates and to steady-state as well as transient

Table 3
Summary statistics of $\log_{10} k$ (m^2) estimated in various ways

Source	Data estimates				Kriging estimates			
	Sample size	Mean	Variance	CV	Sample size	Mean	Variance	CV
Single-hole tests (steady-state analysis)	227	−15.22	0.87	−0.061	53,176	−15.20	0.45	−0.044
Cross-hole tests								
Uniform (equivalent) estimates								
PP4 (type-curve analysis)	30	−13.46	0.34	−0.043	–	–	–	–
PL3, 4, 8, 9, 10, 15 (steady-state analysis)	24	−13.74	0.23	−0.035	–	–	–	–
PP4–PP8 (steady-state analysis)	114	−13.54	0.26	−0.037	–	–	–	–
PL3, 4, 8, 9, 10, 15, PP4–PP8 (steady-state analysis)	138	−13.57	0.26	−0.037	–	–	–	–
Cross-hole tests (numerical inversion)								
Uniform (equivalent) estimates								
PP4	32	−13.57	0.57	−0.056	–	–	–	–
PP4–6	76	−13.70	0.43	−0.048	–	–	–	–
Non-uniform (tomographic) estimates								
PP4: 32 pilot points	–	–	–	–	53,176	−15.23	1.67	−0.085
PP4: 64 pilot points	–	–	–	–	53,176	−14.77	1.62	−0.086
PP4-6: 72 pilot points	–	–	–	–	53,176	−15.69	1.93	−0.089

flow regimes. The scale effect is likewise unrelated to the method of test interpretation: there is consistency between results obtained by means of steady-state analytical formulae from single-hole test data (Guzman et al., 1996), which are shown elsewhere to compare well with transient type-curve (Illman and Neuman, 2000) and inverse (Vesselinov and Neuman, 2001) analyses of the same data, and steady-state as well as type-curve (Illman and Neuman, 2001) and numerical inverse (Vesselinov et al., 2001a,b) interpretations of cross-hole test data. Contrary to a recent suggestion in the literature (Butler and Healey, 1998a,b), the observed scaling behavior is not an artifact of rock conditions around the injection borehole: neither the single-hole (Illman and Neuman, 2000) nor the cross-hole (Illman and Neuman, 2001) test results have been affected by any skin effect of consequence. It is also unrelated to enhanced permeability due to slip flow.

The pronounced permeability scale effect observed at the ALRS is real and amenable to theoretical interpretation (Hyun et al., 2002).

9. Findings and conclusions

Our study leads to the following major findings and conclusions:

1. We found it possible to interpret multiple cross-hole pneumatic injection tests in unsaturated fractured tuffs at the ALRS by means of a steady-state formula based on a linearized version of the non-linear partial differential equation that governs single-phase airflow in a uniform, isotropic porous continuum while treating water as if it was immobile. The formula was developed by Hsieh and Neuman (1985) for hydraulic cross-hole tests in saturated rocks.
2. Steady-state analyses are much easier to conduct than transient type-curve (Illman and Neuman, 2000; Illman and Neuman, 2001) and numerical inverse (Vesselinov and Neuman, 2001; Vesselinov et al., 2001a,b) analyses, which have therefore been limited to relatively few single-hole and cross-hole tests. We found our steady-state approach to work well for pressure records whose signal-to-noise ratio is too low to allow meaningful transient analysis. We were therefore able to augment in a significant way the database previously established for the ALRS by other means. Though the steady-state method does not yield estimates of porosity, it does yield reliable estimates of permeability between an injection and a monitoring interval.
3. Permeability was found by us to vary considerably from one pressure monitoring record to another. Thus, even though our steady-state analysis treats the rock as if it was uniform and isotropic, it ultimately yields information about the spatial variability and directional dependence of permeability across the site.
4. Previous analyses of single-hole and cross-hole pneumatic injection tests have pointed to a pronounced permeability scale effect at the ALRS. The results of our steady-state cross-hole test analyses provide further support for this scale effect by significantly enlarging the corresponding database and eliminating any (previously plausible) suspicion that the cross-hole test data may be biased toward injection into intervals of relatively high permeability.

Acknowledgements

This work was supported in part by the US Nuclear Regulatory Commission under contracts NRC-04-95-038 and NRC-04-97-056. The senior author was also supported by National Science Foundation Graduate Traineeship, the AGU Horton Doctoral Research Grant, a Graduate College Fellowship from the University of Arizona, the John and Margaret Harshbarger Doctoral Fellowship from The University of Arizona as well as the Old Gold Fellowship from the University of Iowa. We thank Bruce Hunt, Xun-Hong Chen, and an anonymous reviewer for their constructive reviews of our manuscript.

References

Baehr, A.L., Hult, M.F., 1991. Evaluation of unsaturated zone air permeability through pneumatic tests. Water Resources Research 27 (10), 2605–2617.

Bassett, R.L., Neuman, S.P., Rasmussen, T.C., Guzman, A., Davidson, G.R., Lohrstorfer, C.F., 1994. In: Woodhouse, E.G.,

(Ed.), Validation Studies for Assessing Unsaturated Flow and Transport Through Fractured Rock, NUREG/CR-6203, US Nuclear Regulatory Commission, Washington, DC.

Benito, P.H., Cook, P.J., Faybishenko, B., Freifeld, B., Doughty, C., 1998. Box Canyon Pneumatic Connectivity Study: Preliminary Data Analysis, Report LBNL-42359, Lawrence Berkeley National Laboratory, Berkeley, CA.

Benito, P.H., Cook, P.J., Faybishenko, B., Freifeld, B., Doughty, C., 1999. Cross-well air-injection packer tests for the assessment of pneumatic connectivity in fractured, unsaturated basalt. In: B., Amadei, R.L., Kranz, G.A., Scott, P.H., Smeallie (Eds.), Proceedings of the 37th US Rock Mechanics Symposium: Rock Mechanics for Industry, 2, pp. 843–850.

Boardman, C.R., Skrove, J., 1966. Distribution in fracture permeability of a granitic rock mass following a contained nuclear explosion. Journal of Petroleum Technology, Petroleum Transactions 18, 619–623.

Butler, J.J. Jr, Healey, J.M., 1998a. Relationship between pumping-test and slug-test parameters: scale effect or artifact? Ground Water 36, 305–313.

Butler, J.J. Jr, Healey, J.M., 1998b. Discussion of papers: authors' reply. Ground Water 36, 867–868.

Chen, G., Illman, W.A., Thompson, D.L., Vesselinov, V.V., Neuman, S.P., 2000. Geostatistical, type curve and inverse analyses of pneumatic injection tests in unsaturated fractured tuffs at the Apache Leap Research Site near Superior, Arizona. In: Faybishenko, B., P.A., Witherspoon, S.M., Benson (Eds.), Dynamics of Fluids in Fractured Rocks, Geophysical Monograph 122, AGU, Washington, DC, pp. 73–98

Chuang, Y., Haldeman, W.R., Rasmussen, T.C., Evans, D.D., 1990. Laboratory Analysis of Fluid Flow and Solute Transport Through a Variably Saturated Fracture Embedded in Porous Tuff, NUREG/CR-5482, US Nuclear Regulatory Commission, Washington, DC.

Edwards, K.B., Jones, L.C., 1994. Air permeability from pneumatic tests in oxidized till. Journal of Environmental Engineering 120 (2), 329–347.

Evans, D.D., Rasmussen, T.C., 1991. Unsaturated Flow and Transport Through Fractured Rock Related to High-Level Waste Repositories, Final Report—Phase III, NUREG/CR-5581, US Nuclear Regulatory Commission, Washington, DC.

Guzman, A.G., Neuman, S.P., 1996. Field air injection experiments. In: Rasmussen, T.C., Rhodes, S.C., Guzman, A., Neuman, S.P. (Eds.), Apache Leap Tuff INTRAVAL Experiments: Results and Lessons Learned, NUREG/CR-6096, US Nuclear Regulatory Commission, Washington, DC, pp. 52–91.

Guzman, A.G., Neuman, S.P., Lohrstorfer, C.F., Bassett, R., 1994. Field hydraulic, pneumatic, and tracer tests. In: Bassett, R.L., Neuman, S.P., Rasmussen, T.C., Guzman, A.G., Davidson, G.R., Lohrstorfer, C.F. (Eds.), Validation Studies for Assessing Unsaturated Flow and Transport Through Fractured Rock, NUREG/CR-6203, US Nuclear Regulatory Commission, Washington, DC, pp. 4-1–4-58.

Guzman, A.G., Geddis, A.M., Henrich, M.J., Lohrstorfer, C.F., Neuman, S.P., 1996. Summary of Air Permeability Data from Single-Hole Injection Tests in Unsaturated Fractured Tuffs at the Apache Leap Research Site: Results of Steady-State Test Interpretation, NUREG/CR-6360, US Nuclear Regulatory Commission, Washington, DC.

Haldeman, W.R., Chuang, Y., Rasmussen, T.C., Evans, D.D., 1991. Laboratory analysis of fluid flow and solute transport through a fracture embedded in porous tuff. Water Resources Research 27 (1), 53–65.

Hsieh, P.A., Neuman, S.P., 1985. Field determination of the three-dimensional hydraulic conductivity tensor of anisotropic media. 1. Theory. Water Resources Research 21 (11), 1655–1665.

Hsieh, P.A., Neuman, S.P., Stiles, G.K., Simpson, E.S., 1985. Field determination of the three-dimensional hydraulic conductivity tensor of anisotropic media. 2. Methodology and application to fractured rocks. Water Resources Research 21 (11), 1667–1676.

Huang, K., Tsang, Y.W., Bodvarsson, G.S., 1999. Simultaneous inversion of air-injection tests in fractured unsaturated tuff at Yucca Mountain. Water Resources Research 35 (8), 2375–2386.

Hyun, Y., Neuman, S.P., Vesselinov, V.V., Illman, W.A., Tartakovsky, D.M., Di Federico, V., 2001. Theoretical interpretation of a pronounced permeability scale-effect in unsaturated fractured tuff. Water Resources Research 38 (6) 101029/R000658.

Illman, W.A., 1999. Single- and cross-hole pneumatic injection tests in unsaturated fractured tuffs at the Apache Leap Research Site near Superior, Arizona. PhD Dissertation, Department of Hydrology and Water Resources, University of Arizona, Tucson.

Illman, W.A., Neuman, S.P., 2000. Type-curve interpretation of multi-rate single-hole pneumatic injection tests in unsaturated fractured rock. Ground Water 38 (6), 899–911.

Illman, W.A., Neuman, S.P., 2001. Type-curve interpretation of a cross-hole pneumatic test in unsaturated fractured tuff. Water Resources Research 37 (3), 583–604.

Illman, W.A., Thompson, D.L., Vesselinov, V.V., Chen, G., Neuman, S.P., 1998. Single- and Cross-Hole Pneumatic Tests in Unsaturated Fractured Tuffs at the Apache Leap Research Site: Phenomenology, Spatial Variability, Connectivity and Scale, NUREG/CR-5559, US Nuclear Regulatory Commission, Washington, DC.

Kirkham, D., 1946. Field method for determination of air permeability of soil in its undisturbed state. Soil Science Society of America, Proceedings 11, 93–99.

Klinkenberg, L.J., 1941. The permeability of porous media to liquids and gases. American Petroleum Institute, Drilling and Production Practice, 200–213.

LeCain, G.D., 1995. Pneumatic testing in 45-degree-inclined boreholes in ash-flow tuff near Superior, Arizona. US Geological Survey Water-Resources Investigations Report 95-4073.

LeCain, G.D., 1996. Air-injection testing in vertical boreholes in welded and nonwelded tuff, Yucca Mountain, Nevada. US Geological Survey Water-Resources Investigations Report 96-4262.

LeCain, G.D., 1998. Results from air-injection and tracer testing in the Upper Tiva Canyon, Bow Ridge Fault, and Upper Paintbrush Contact Alcoves of the Exploratory Studies Facility, August

1994 through July 1996, Yucca Mountain, Nevada. Water-Resources Investigations Report 98-4058.

LeCain, G.D., Walker, J.N., 1994. Results of air-permeability testing in a vertical borehole at Yucca Mountain, Nevada, Proceedings of the Fifth Annual International Conference on High-Level Radioactive Waste Management, Las Vegas, NV, May 22–26, pp. 2782–2788.

Massmann, J.W., Madden, M., 1994. Estimating air conductivity and porosity from vadose-zone pumping tests. Journal of Environmental Engineering 120 (2), 313–328.

Mishra, S., Bodvarsson, G.S., Attanayake, M.P., 1987. Injection and falloff test analysis to estimate properties of unsaturated fractures. In: Evans, D.D., Nicholson, T.J. (Eds.), Flow and Transport through Unsaturated Fractured Rock, American Geophysical Union, Geophysical Monograph 42, pp. 149–156.

Montazer, P.M., 1982. Permeability of unsaturated fractured metamorphic rocks near an underground opening. PhD Dissertation, Colorado School of Mines, Golden, CO.

Neuman, S.P., 1987. Stochastic continuum representation of fractured rock permeability as an alternative to the REV and fracture network concepts. In: Farmer, I.W., Daemen, J.J.K., Desai, C.S., Glass, C.E., Neuman, S.P. (Eds.), Rock Mechanics: Proceedings of the 28th US Symposium, Tucson, Arizona, A.A. Balkema, Rotterdam, pp. 533–561, 1240 pp. Also pp. 331–362. Custodio, E., Gurgui, A., Lobo Ferreira, J.P. (Eds.), 1988. Groundwater Flow and Quality Modelling. NATO ASI Series C, 224. D. Reidel, Dordrecht, Holland. 843 pp.

Peterson, D.W., 1961. Dacitic ash-flow sheet near Superior and Globe, Arizona. PhD Dissertation, Stanford University, Palo Alto, CA.

Rasmussen, T.C., Evans, D.D., 1987. Unsaturated Flow and Transport through Fractured Rock-Related to High-level Waste Repositories, Final Report—Phase II, NUREG/CR-4655, US Nuclear Regulatory Commission, Washington DC.

Rasmussen, T.C., Evans, D.D., 1989. Fluid Flow and Solute Transport Modeling through Three-Dimensional Networks of Variably Saturated Discrete Fractures, NUREG/CR-5239, US Nuclear Regulatory Commission, Washington, DC.

Rasmussen, T.C., Evans, D.D., 1992. Nonisothermal Hydrologic Transport Experimental Plan, NUREG/CR-5880, US Nuclear Regulatory Commission, Washington, DC.

Rasmussen, T.C., Evans, D.D., Sheets, P.J., Blanford, J.H., 1990. Unsaturated Fractured Rock Characterization Methods and Data Sets at the Apache Leap Tuff Site, NUREG/CR-5596, US Nuclear Regulatory Commission, Washington, DC.

Rasmussen, T.C., Evans, D.D., Sheets, P.J., Blanford, J.H., 1993. Permeability of Apache Leap Tuff: borehole and core measurements using water and air. Water Resources Research 29 (7), 1997–2006.

Rasmussen, T.C., Rhodes, S.C., Guzman, A., Neuman, S.P., 1996. Apache Leap Tuff INTRAVAL Experiments: Results and Lessons Learned, NUREG/CR-6096, US Nuclear Regulatory Commission, Washington, DC.

Tidwell, V.C., Rasmussen, T.C., Evans, D.D., 1988. Saturated hydraulic conductivity estimates for fractured rocks in the unsaturated zone. In: Wierenga, P.J., (Ed.), Proceedings of International Conference and Workshop on the Validation of Flow and Transport Models for the Unsaturated Zone, New Mexico State University, Las Cruces, NM.

Trautz, R.C., 1984. Rock fracture aperture and gas conductivity measurements in-situ. MS Thesis, Department of Hydrology and Water Resources, University of Arizona, Tucson.

Vesselinov, V.V., 2000, Numerical inverse interpretation of pneumatic tests in unsaturated fractured tuffs at the Apache Leap Research Site. PhD Dissertation, Department of Hydrology and Water Resources, University of Arizona, Tucson.

Vesselinov, V.V., Neuman, S.P., 2001. Numerical inverse interpretation of single-hole pneumatic tests in unsaturated fractured tuff. Ground Water 39 (5), 685–695.

Vesselinov, V.V., Neuman, S.P., Illman, W.A., 2001a. Three-dimensional numerical inversion of pneumatic cross-hole tests in unsaturated fractured tuff. 1. Methodology and borehole effects. Water Resources Research 37 (12), 3001–3017.

Vesselinov, V.V., Neuman, S.P., Illman, W.A., 2001b. Three-dimensional numerical inversion of pneumatic cross-hole tests in unsaturated fractured tuff. 2. Equivalent parameters, high-resolution stochastic imaging and scale effects. Water Resources Research 37 (12), 3019–3041.

Vickers, B.C., Neuman, S.P., Sully, M.J., Evans, D.D., 1992. Reconstruction and geostatistical analysis of multiscale fracture apertures in a large block of welded tuff. Geophysical Research Letters 19 (10), 1029–1032.

Wang, J.S.Y., Cook, P.J., Trautz, R.C., Salve, R., James, A.L., Finsterle, S., Tokunaga, T.K., Solbau, R., Clyde, J., Flint, A.L., Flint, L.E., 1998. Field testing and observation of flow paths in niches: phase 1 status report of the drift seepage test and niche moisture study: Yucca Mountain Project Milestone SPC314M4, Lawrence Berkeley National Laboratory, Berkeley, CA.

Weber, D.S., Evans, D.D., 1988. Stable Isotopes of Authigenic Minerals in Variably-Saturated Fractured Tuff, NUREG/CR-5255, US Nuclear Regulatory Commission, Washington, DC.

Yeh, T.C., Rasmussen, T.C., Evans, D.D., 1988. Simulation of Liquid and Vapor Movement in Unsaturated Fractured Rock at the Apache Leap Tuff Site—Models and Strategies, NUREG/CR-5097, US Nuclear Regulatory Commission, Washington, DC.